Research Article | Vol. 25, No. 24 | 27 Nov 2017 | OPTICS EXPRESS 29687

Optics EXPRESS

Optical Peregrine rogue waves of self-induced transparency in a resonant erbium-doped fiber

SHIHUA CHEN,[1,*] YANLIN YE,[1] FABIO BARONIO,[2,5] YI LIU,[3] XIAN-MING CAI,[1] AND PHILIPPE GRELU [4,6]

[1]*Department of Physics, Southeast University, Nanjing 211189, China*
[2]*INO CNR and Dipartimento di Ingegneria dell'Informazione, Università di Brescia, Via Branze 38, 25123 Brescia, Italy*
[3]*Shanghai Key Lab of Modern Optical System, University of Shanghai for Science and Technology, 516, Jungong Road, 200093 Shanghai, China*
[4]*Laboratoire Interdisciplinaire Carnot de Bourgogne, U.M.R. 6303 C.N.R.S., Université Bourgogne Franche-Comté, 9 avenue A. Savary, F-21078 Dijon, France*
[5]*fabio.baronio@unibs.it*
[6]*philippe.grelu@u-bourgogne.fr*
[*]*cshua@seu.edu.cn*

Abstract: The resonant interaction of an optical field with two-level doping ions in a cryogenic optical fiber is investigated within the framework of nonlinear Schrödinger and Maxwell-Bloch equations. We present explicit fundamental rational rogue wave solutions in the context of self-induced transparency for the coupled optical and matter waves. It is exhibited that the optical wave component always features a typical Peregrine-like structure, while the matter waves involve more complicated yet spatiotemporally balanced amplitude distribution. The existence and stability of these rogue waves is then confirmed by numerical simulations, and they are shown to be excited amid the onset of modulation instability. These solutions can also be extended, using the same analytical framework, to include higher-order dispersive and nonlinear effects, highlighting their universality.

OCIS codes: (190.3100) Instabilities and chaos; (190.5530) Pulse propagation and temporal solitons; (190.4370) Nonlinear optics, fibers.

References and links

1. C. Kharif, E. Pelinovsky, and A. Slunyaev, *Rogue Waves in the Ocean* (Springer, 2009).
2. M. Onorato, S. Residori, U. Bortolozzo, A. Montina, and F. T. Arecchi, "Rogue waves and their generating mechanisms in different physical contexts," Phys. Rep. **528**, 47–89 (2013).
3. A. Chabchoub, N. P. Hoffmann, and N. Akhmediev, "Rogue wave observation in a water wave tank," Phys. Rev. Lett. **106**, 204502 (2011).
4. H. Bailung, S. K. Sharma, and Y. Nakamura, "Observation of Peregrine solitons in a multicomponent plasma with negative ions," Phys. Rev. Lett. **107**, 255005 (2011).
5. D. R. Solli, C. Ropers, P. Koonath, and B. Jalali, "Optical rogue waves," Nature (London) **450**, 1054–1057 (2007).
6. B. Kibler, J. Fatome, C. Finot, G. Millot, F. Dias, G. Genty, N. Akhmediev, and J. M. Dudley, "The Peregrine soliton in nonlinear fibre optics," Nature Phys. **6**, 790–795 (2010).
7. C. Lecaplain, Ph. Grelu, J. M. Soto-Crespo, and N. Akhmediev, "Dissipative rogue waves generated by chaotic pulse bunching in a mode-locked laser," Phys. Rev. Lett. **108**, 233901 (2012).
8. B. Frisquet, B. Kibler, Ph. Morin, F. Baronio, M. Conforti, G. Millot, and S. Wabnitz, "Optical dark rogue wave," Sci. Rep. **6**, 20785 (2016).
9. Yu. V. Bludov, V. V. Konotop, and N. Akhmediev, "Matter rogue waves," Phys. Rev. A **80**, 033610 (2009).
10. S. Chen, F. Baronio, J. M. Soto-Crespo, Ph. Grelu, and D. Mihalache, "Versatile rogue waves in scalar, vector, and multidimensional nonlinear systems," J. Phys. A **50**, 463001 (2017).
11. N. Akhmediev, A. Ankiewicz, and M. Taki, "Waves that appear from nowhere and disappear without a trace," Phys. Lett. A **373**, 675–678 (2009).
12. J. M. Dudley, F. Dias, M. Erkintalo, and G. Genty, "Instabilities, breathers and rogue waves in optics," Nature Photon. **8**, 755–764 (2014).
13. D. H. Peregrine, "Water waves, nonlinear Schödinger equations and their solutions," J. Aust. Math. Soc. Series B: Appl. Math. **25**, 16–43 (1983).

#309622 https://doi.org/10.1364/OE.25.029687
Journal © 2017 Received 20 Oct 2017; revised 7 Nov 2017; accepted 7 Nov 2017; published 13 Nov 2017

Optics EXPRESS

14. N. Akhmediev, B. Kibler, F. Baronio, M. Belić, W.-P. Zhong, Y. Zhang, W. Chang, J. M. Soto-Crespo, P. Vouzas, Ph. Grelu, C. Lecaplain, K. Hammani, S. Rica, A. Picozzi, M. Tlidi, K. Panajotov, A. Mussot, A. Bendahmane, P. Szriftgiser, G. Genty, J. Dudley, A. Kudlinski, A. Demircan, U. Morgner, S. Amiraranashvili, C. Bree, G. Steinmeyer, C. Masoller, N. G. R. Broderick, A. F. J. Runge, M. Erkintalo, S. Residori, U. Bortolozzo, F. T. Arecchi, S. Wabnitz, C. G. Tiofack, S. Coulibaly, and M. Taki, "Roadmap on optical rogue waves and extreme events", J. Opt. **18**, 063001 (2016).
15. A. Ankiewicz, J. M. Soto-Crespo, and N. Akhmediev, "Rogue waves and rational solutions of the Hirota equation," Phys. Rev. E **81**, 046602 (2010).
16. S. Chen, "Twisted rogue-wave pairs in the Sasa-Satsuma equation," Phys. Rev. E **88**, 023202 (2013).
17. A. Ankiewicz, D. J. Kedziora, A. Chowdury, U. Bandelow, and N. Akhmediev, "Infinite hierarchy of nonlinear Schrödinger equations and their solutions," Phys. Rev. E **93**, 012206 (2016).
18. S. Chen, F. Baronio, J. M. Soto-Crespo, Y. Liu, and Ph. Grelu, "Chirped Peregrine solitons in a class of cubic-quintic nonlinear Schrödinger equations," Phys. Rev. E **93**, 062202 (2016).
19. F. Baronio, A. Degasperis, M. Conforti, and S. Wabnitz, "Solutions of the vector nonlinear Schrödinger equations: Evidence for deterministic rogue waves," Phys. Rev. Lett. **109**, 044102 (2012).
20. J. He, S. Xu, and K. Porseizan, "N-order bright and dark rogue waves in a resonant erbium-doped fiber system," Phys. Rev. E **86**, 066603 (2012).
21. F. Baronio, M. Conforti, A. Degasperis, and S. Lombardo, "Rogue waves emerging from the resonant interaction of three waves," Phys. Rev. Lett. **111**, 114101 (2013).
22. S. Chen, J. M. Soto-Crespo, and Ph. Grelu, "Coexisting rogue waves within the (2+1)-component long-wave–short-wave resonance," Phys. Rev. E **90**, 033203 (2014).
23. F. Baronio, M. Conforti, A. Degasperis, S. Lombardo, M. Onorato, and S. Wabnitz, "Vector rogue waves and baseband modulation instability in the defocusing regime," Phys. Rev. Lett. **113**, 034101 (2014).
24. S. Chen, J. M. Soto-Crespo, and Ph. Grelu, "Dark three-sister rogue waves in normally dispersive optical fibers with random birefringence," Opt. Express **22**(22), 27632–27642 (2014).
25. S. Chen and D. Mihalache, "Vector rogue waves in the Manakov system: Diversity and compossibility," J. Phys. A: Math. Theor. **48**, 215202 (2015).
26. H. A. Haus, "Physical interpretation of inverse scattering formalism applied to self-induced transparency," Rev. Mod. Phys. **51**, 331–339 (1979).
27. R. W. Ziolkowski, J. M. Arnold, and D. M. Gogny, "Ultrafast pulse interactions with two-level atoms," Phys. Rev. A **52**, 3082–3094 (1995).
28. G. H. M. van Tartwijk and G. P. Agrawal, "Maxwell–Bloch dynamics and modulation instabilities in fiber lasers and amplifiers," J. Opt. Soc. Am. B **14**(10), 2618–2627 (1997).
29. Q.-H. Park and R. W. Boyd, "Modification of self-induced transparency by a coherent control field," Phys. Rev. Lett. **86**, 2774–2777 (2001).
30. S. L. McCall and E. L. Hahn, "Self-induced transparency by pulsed coherent light," Phys. Rev. Lett. **18**, 908–911 (1967).
31. L. Allen and J. H. Eberly, *Optical Resonance and Two-Level Atoms* (Wiley, 1975).
32. R. M. Arkhipov, M. V. Arkhipov, I. Babushkin, and N. N. Rosanov, "Self-induced transparency mode locking, and area theorem," Opt. Lett. **41**(4), 737–740 (2016).
33. D. J. Kaup, A. Reiman, and A. Bers, "Space-time evolution of nonlinear three-wave interactions. I. Interaction in a homogeneous medium," Rev. Mod. Phys. **51**, 275–309 (1979).
34. E. Ibragimov and A. Struthers, "Second-harmonic pulse compression in the soliton regime," Opt. Lett. **21**(19), 1582–1584 (1996).
35. M. Conforti, F. Baronio, A. Degasperis, and S. Wabnitz, "Inelastic scattering and interactions of three-wave parametric solitons," Phys. Rev. E **74**, 065602(R) (2006).
36. F. Baronio, M. Conforti, C. De Angelis, A. Degasperis, M. Andreana, V. Couderc, and A. Barthélémy, "Velocity-locked solitary waves in quadratic media," Phys. Rev. Lett. **104**, 113902 (2010).
37. S. Chen, J. M. Soto-Crespo, and Ph. Grelu, "Watch-hand-like optical rogue waves in three-wave interactions," Opt. Express **23**(1), 349–359 (2015).
38. S. Chen, F. Baronio, J. M. Soto-Crespo, Ph. Grelu, M. Conforti, and S. Wabnitz, "Optical rogue waves in parametric three-wave mixing and coherent stimulated scattering," Phys. Rev. A **92**, 033847 (2015).
39. S. Chen, X.-M. Cai, Ph. Grelu, J. M. Soto-Crespo, S. Wabnitz, and F. Baronio, "Complementary optical rogue waves in parametric three-wave mixing," Opt. Express **24**(6), 5886–5895 (2016).
40. M. Nakazawa, E. Yamada, and H. Kubota, "Coexistence of a self-induced-transparency soliton and a nonlinear Schrödinger soliton in an erbium-doped fiber," Phys. Rev. A **44**, 5973–5987 (1991).
41. M. Nakazawa, Y. Kimura, K. Kurokawa, and K. Suzuki, "Self-induced-transparency solitons in an erbium-doped fiber waveguide," Phys. Rev. A **45**, R23–R26 (1992).
42. A. I. Maimistov and E. A. Manykin, "Propagation of ultrashort optical pulses in resonant nonlinear light guides," Zh. Eksp. Teor. Fiz. **85**, 1177–1181 (1983).
43. J. S. He, Y. Cheng, and Y. S. Li, "The Darboux transformation for NLS-MB equations," Commun. Theor. Phys. **38**, 493–496 (2002).
44. C. Li, J. He, and K. Porsezian, "Rogue waves of the Hirota and the Maxwell-Bloch equations," Phys. Rev. E **87**,

Optics EXPRESS

012913 (2013).
45. F. Baronio, S. Chen, Ph. Grelu, S. Wabnitz, and M. Conforti, "Baseband modulation instability as the origin of rogue waves," Phys. Rev. A **91**, 033804 (2015).
46. B. Kleefeld, A. Q. M. Khaliq, and B. A. Wade, "An ETD Crank-Nicolson method for reaction-diffusion systems," Numer. Methods PDEs **28**, 1309–1335 (2012).
47. A. Hasegawa, Y. Kodama, and A. Maruta, "Recent progress in dispersion-managed soliton transmission technologies," Opt. Fiber Technol. **3**, 197–213 (1997).
48. K. Goda and B. Jalali, "Dispersive Fourier transformation for fast continuous single-shot measurements," Nature Photon. **7**, 102–112 (2013).

1. Introduction

Since its coming forth in oceanography [1], the concept of rogue waves has rapidly and profoundly penetrated into most branches of physics as diverse as hydrodynamics [2, 3], plasma physics [4], nonlinear optics [5–8], and Bose-Einstein condensation [9]. This great success is the result of the fundamental interest on one side, and the multidisciplinary diffusion of soliton concept a few decades ago on the other side, as both solitons and rogue waves are associated to the integrability of a class of nonlinear wave equations and generally share the same Darboux transformation [10]. Compared to the stationary solitons, rogue waves are modeled as transient wave-packets localized in both space and time, to mimic the episodic giants that seemingly appear from nowhere and disappear without a trace [11]. In a broad sense, rogue waves are frequently termed as rational solitons on a finite background [12], for instance, the so-called "Peregrine soliton" represents actually the archetypal rogue wave waveform [13].

Rogue wave research flourishes now in both theoretical and experimental aspects [10, 12, 14], providing novel perspectives for the manifestation of extreme waves in a variety of nonlinear media. To reflect the diversity and complexity of media, it requires the study of the propagation models that go beyond the scalar nonlinear Schrödinger (NLS) equation, such as the extended scalar models [15–18] and the coupled multicomponent models [19–25].

The interaction of optical pulses with nonlinear resonant media is a long-standing topic of research in optics. As a central figure, the resonant interaction of pulses with two-level atoms or ions yields the thoroughly studied Maxwell-Bloch (MB) system of light-matter coupled equations [26–29]. Within such light-matter interaction, an otherwise absorbing material becomes completely transparent for optical pulses of duration shorter than all the relevant relaxation times of the medium. This phenomenon is known as self-induced transparency (SIT) [30], and can yield a fundamental sech-shaped soliton of area 2π [31, 32]. It has recently been shown theoretically to admit rogue wave solutions [20]. An interesting comparison may be drawn between this MB coupling and the parametric three-wave resonant interaction (TWRI) occurring in weakly dispersive *non-resonant* media [33, 34]. For the latter case, three field components are involved, which respect momentum and energy conservation during interaction. They admit as well coherent localized structures such as solitons [35, 36] and rogue waves [37–39].

In this paper, we revisit the rogue wave formation in the quasi-resonant optical-driven two-level system, within the NLS–MB framework [40, 41], which generalizes the above MB case by including the group-velocity dispersion (GVD) and the Kerr nonlinearity. By providing for the first time a universal explicit analytical expression of the coupled multicomponent rogue wave solutions, we unveil further the relationship between matter and optical rogue waves, and numerically confirm their stability in spite of the onset of modulation instability (MI). Considering the future possibility of observation of these rogue waves in a laboratorial environment, we also provide a clearer access to the parameters needed for experimental design.

2. Theoretical framework

We suppose that a linearly-polarized optical field propagates in a single-mode ion-doped glass fiber. These ions are considered as independent two-level doping centers interacting with the

Optics EXPRESS

electric field component, expressed as $E(x,y,z,t) = \frac{1}{2}\hat{x}B(x,y)u(z,t)\exp(i\beta_0 z - i\omega_0 t) + c.c.$, whose carrier frequency ω_0 is close to the resonance frequency ω_{21} of the transition between the two levels. Here $\hat{x}$ is the polarization unit vector along the x-axis, $B(x,y)$ is the fiber-mode profile, $u(z,t)$ is the complex envelope in the physical unit $\sqrt{\mathrm{W}}$, $\beta_0 = k(\omega_0)$ is the wave number at the carrier frequency, and $c.c.$ means the complex conjugate. In general, the propagation of the electric field in such a medium will be ruled by a non-integrable MB or NLS-MB equation set [28], due to the presence of damping terms accounting for the spontaneous emission and matter-wave dipole decays. However, it is conceivable to study propagation phenomena characterized by time scales shorter than the dipole and population decay times, providing a solvable model for the investigation of SIT. The latter represents our theoretical framework.

Therefore, using the slowly-varying envelope and rotating-wave approximations, the propagation of the electric field in an ion-doped optical fiber can be governed by the following coupled NLS–MB equations [26,40,41]:

$$\begin{aligned} &iu_z - \frac{\beta_2}{2}u_{tt} + \gamma|u|^2u + \frac{\hbar R\Omega^2 n}{2cp_{21}}\langle v_1 v_2^*\rangle = 0,\\ &v_{1t} = \frac{i}{2}\delta v_1 + \frac{2ip_{21}}{\hbar R}uv_2,\\ &v_{2t} = -\frac{i}{2}\delta v_2 + \frac{2ip_{21}^*}{\hbar R}u^*v_1, \end{aligned} \tag{1}$$

where $v_1(z,t)$ and $v_2(z,t)$ are the matter wave functions for the lower (1) and upper (2) levels, respectively, depending on the propagation distance z and retarded time t. Here by *matter waves* we mean the state functions of the matter considered static, in contrast to traveling de Broglie waves. As the total probability of finding a dopant atom in either the upper or lower levels is equal to unity, the matter wave functions must satisfy $|v_1|^2 + |v_2|^2 = 1$. The subscripts stand for partial derivatives, and the asterisks and brackets denote complex conjugation and a local average over two-level systems, respectively. $\delta = \omega_0 - \omega_{21}$ is the laser detuning to resonance, $\hbar$ is the Planck constant divided by 2π, c is the speed of light in vacuum, n is the linear refractive index of medium, and $p_{21} = p_{12}^*$ is the complex dipole matrix element of transition between upper and lower states. The coefficients $\beta_2 = \frac{d^2k(\omega)}{d\omega^2}|_{\omega=\omega_0}$ and $\gamma = \frac{n_2\omega_0}{cA_{\mathrm{eff}}} > 0$ account for the GVD and Kerr nonlinearity of the host fiber, respectively, with n_2 the nonlinear refractive index, and A_{eff} the cross section of the spatial guided mode. Besides, we have defined the characteristic frequency $\Omega = \sqrt{\frac{\omega_0 N|p_{21}|^2}{2\hbar\varepsilon_0 n^2}}$ and the scaling factor $R = \sqrt{\varepsilon_0 cnA_{\mathrm{eff}}/2}$, where ϵ_0 is the permittivity of free space, and N is the concentration of two-level doping centers.

We need to point out that Eqs. (1) are also termed the SIT-NLS equations [40]. They constitute a peculiar vector system, since only the electric field truly propagates along the z direction, whereas the matter-wave evolutions are each expressed by a first-order derivative with respect to t. This is a fundamental difference between this vector system and those composed of coupled optical waves, such as the TWRI system mentioned earlier [35,36].

As in most NLS frameworks, considering that the normal dispersion case ($\beta_2 > 0$) precludes any valid rogue wave solutions, we confine our discussion to the anomalous dispersion $\beta_2 < 0$. By virtue of the following transformations of variables

$$A = \frac{u}{\sqrt{P_{\mathrm{SIT}}}}, \quad M = \frac{2i|p_{21}|}{p_{21}\sqrt{\sigma}}v_1 v_2^*, \quad F = |v_2|^2 - |v_1|^2, \quad \xi = \frac{z}{z_s}, \quad \text{and} \quad \tau = \frac{t}{\tau_s}, \tag{2}$$

the coupled Eqs. (1) can be normalized to the dimensionless form

$$A_\xi = i(\frac{\sigma}{2}A_{\tau\tau} + \frac{P_{\mathrm{SIT}}}{P_{\mathrm{NLS}}}|A|^2A) + \langle M\rangle, \quad M_\tau = i\phi M - \frac{2}{\sigma}AF, \quad F_\tau = M^*A + MA^*, \tag{3}$$

Optics EXPRESS

where τ_s is a typical pulse duration, which defines the unit time scale, $\phi = \delta\tau_s$ is the scaled laser detuning, $P_{\rm NLS} = \frac{1}{z_s\gamma}$ is the peak power of the usual NLS soliton, and $P_{\rm SIT} = \frac{\hbar^2 R^2}{4\sigma\tau_s^2|p_{21}|^2}$ denotes the peak power of the SIT soliton when the NLS component is absent, with

$$z_s = \frac{2c}{\sigma n\tau_s\Omega^2}, \quad z_d = \frac{\tau_s^2}{|\beta_2|}, \quad \text{and} \quad \sigma = \frac{z_s}{z_d} = \frac{1}{\Omega}\sqrt{\frac{2c}{n\tau_s z_d}}, \tag{4}$$

being the SIT length, the dispersion length, and the scaled dispersion, respectively. We note that, while M is related to the off-diagonal element ρ_{12}, $F = \rho_{22} - \rho_{11}$ signifies the local population difference between the upper and lower levels, where $\rho_{ij} = v_i v_j^*$ denotes the element of the density matrix describing the resonant atom-like systems [26]. Therefore, the condition of probability conservation mentioned above can be rewritten as

$$F^2 + \sigma|M|^2 = 1. \tag{5}$$

On the other hand, for a specific line-shape function $g(\phi)$, one can calculate the average $\langle M\rangle$ in the first of Eqs. (3) according to

$$\langle M\rangle = \int_{-\infty}^{\infty} M(\xi,\tau,\phi')g(\phi')d\phi'. \tag{6}$$

For the sake of simplicity, we will assume below the line shape to be of Dirac delta type, i.e., $g(\phi') = \delta(\phi - \phi')$, which is true when the Lorentzian line profile (homogeneous broadening) or Gaussian line profile (inhomogeneous broadening) has an infinitesimal scale parameter. Under such circumstances, it follows then that $\langle M\rangle = M$.

3. Integrable NLS-MB model and exact rogue wave solutions

It is now evident that as the condition

$$P_{\rm NLS} = P_{\rm SIT}, \quad \text{or equivalently,} \quad \gamma = \frac{4|p_{21}|^2|\beta_2|}{\hbar^2 R^2}, \tag{7}$$

is met [40, 42], Eqs. (3) can be reduced to the integrable form

$$A_\xi = is(\frac{\sigma}{2}A_{\tau\tau} + |A|^2 A) + M, \qquad M_\tau = i\phi M - \frac{2}{\sigma}AF, \qquad F_\tau = M^*A + MA^*, \tag{8}$$

where for the sake of discussion, we have introduced the parameter s to separate the MB equations ($s = 0$) from the NLS-MB equations ($s = 1$).

We follow the standard Darboux transformation procedure as in [20, 43], and obtain the fundamental rational solutions of Eqs. (8) as

$$A(\xi,\tau) = A_0\left(1 - \frac{16i\eta\xi + 4}{16\eta^2\xi^2 + 4a^2\theta^2/\sigma + 1}\right), \tag{9}$$

$$M(\xi,\tau) = M_0\left\{1 - \frac{4i\kappa^2(4\eta\xi - i)}{(\kappa^2 + 4\sigma a^2)(16\eta^2\xi^2 + 4a^2\theta^2/\sigma + 1)} - \frac{64i[4a^2\theta^2 + \sigma(4\eta\xi - i)^2]a^2\eta\xi + 32(4\eta\xi - i)a^2\kappa\theta}{(\kappa^2 + 4\sigma a^2)(16\eta^2\xi^2 + 4a^2\theta^2/\sigma + 1)^2}\right\}, \tag{10}$$

$$F(\xi,\tau) = \frac{\kappa b}{2a} - \frac{8\sigma ab[(16\eta^2\xi^2 - 4a^2\theta^2/\sigma + 1)\kappa - 32a^2\eta\xi\theta]}{(\kappa^2 + 4\sigma a^2)(16\eta^2\xi^2 + 4a^2\theta^2/\sigma + 1)^2}, \tag{11}$$

where

$$\kappa = \sigma(\omega - \phi), \qquad \theta = \tau - \sigma\chi\xi, \tag{12}$$

Optics EXPRESS

$$\eta = -\frac{\sigma a b}{\kappa^2 + 4\sigma a^2} + \frac{s a^2}{2}, \quad \chi = \frac{\kappa b}{a(\kappa^2 + 4\sigma a^2)} + s\omega. \tag{13}$$

The initial plane-wave seeds $A_0(\xi, \tau)$, $M_0(\xi, \tau)$, and $F_0(\xi, \tau)$ are defined by

$$A_0 = a \exp\left[i\left(K\xi + \omega\tau\right)\right], \quad M_0 = i\frac{b}{a}A_0, \quad F_0 = \frac{\kappa b}{2a}, \tag{14}$$

with the dispersion relation

$$K = \frac{b}{a} + s(a^2 - \frac{\sigma\omega^2}{2}). \tag{15}$$

It is easy to show that, for given solution forms (10) and (11), the spatiotemporal distributions of F and M always satisfy

$$F(\xi, \tau)^2 + \sigma|M(\xi, \tau)|^2 = (\frac{\kappa^2}{4a^2} + \sigma)b^2, \tag{16}$$

suggesting that the matter-wave components are endowed with a complementary rogue wave property similar to that obtained for the degenerate TWRI system [39].

Let us pay more attention on these solutions, which basically hold true for arbitrary b values. However, only two special values of b are physically relevant. To be specific, as $b = 0$, the optical field A still takes the nontrivial Peregrine form (9), but the matter-wave functions M and F become nil, as seen from Eqs. (10) and (11). In this case, the vector model (8) is decoupled to the single scalar NLS equation, and correspondingly, its rational solution (9) can be identified as an NLS-Peregrine soliton [13] because the matter-wave effects are absent now. Once the matter waves are initiated, according to Eqs. (5) and (16), the b value should be given by

$$b = \frac{2a}{\sqrt{\kappa^2 + 4\sigma a^2}}, \tag{17}$$

which is dependent on the parameters a, κ, and σ. In such an SIT case, one can term the solution (9) as the SIT-Peregrine soliton to make it different from that obtained with $b = 0$.

In addition, one may notice that the solutions (9)–(11) are applicable for either $\sigma > 0$ or $\sigma < 0$. However, in the latter situation (i.e., in the normal dispersion regime), these solutions will become singular and thus could not occur in practice. This is the reason why only the anomalous dispersion was taken into account in the paper.

4. Intriguing rogue wave dynamics

We find from solutions (9)–(11) that, while the optical field A always takes the form of typical Peregrine soliton [13], M and F involve polynomials of fourth order, hence exhibiting more complex structures that are spatiotemporally balanced in amplitude distributions, namely, $F(\xi, \tau)^2 + \sigma|M(\xi, \tau)|^2 = 1$. A closer inspection of Eq. (10) reveals that $|M|$ usually possesses four holes that fall to zero in the dip center. These four hole positions, at which the amplitude is vanishing, i.e., $|M(\xi_0,\ \tau_0)| = 0$, are found to be

$$\xi_0 = \pm\frac{\sqrt{2}}{8\eta}\left(\frac{4\sigma a^2 - \kappa^2}{4\sigma a^2 + \kappa^2} + \sqrt{\frac{\kappa^2}{4\sigma a^2 + \kappa^2}}\right)^{1/2}, \quad \tau_0 = \sigma\chi\xi_0 + \frac{4\sigma\eta\xi_0|\kappa|/\kappa}{\sqrt{4\sigma a^2 + \kappa^2} - |\kappa|}, \tag{18}$$

and

$$\xi_0 = \pm\frac{\sqrt{2}}{8\eta}\left(\frac{4\sigma a^2 - \kappa^2}{4\sigma a^2 + \kappa^2} - \sqrt{\frac{\kappa^2}{4\sigma a^2 + \kappa^2}}\right)^{1/2}, \quad \tau_0 = \sigma\chi\xi_0 - \frac{4\sigma\eta\xi_0|\kappa|/\kappa}{\sqrt{4\sigma a^2 + \kappa^2} + |\kappa|}. \tag{19}$$

Optics EXPRESS

It is worth noting that while the former two holes defined by Eq. (18) always exist, the latter two given by Eq. (19) would vanish as $|\kappa| > \frac{2\sqrt{3\sigma a}}{3}$. It is easy to show that at these extremal positions, the population difference F must satisfy $F(\xi_0,\ \tau_0) = \pm 1$.

Take the simplest MB case ($s = 0$) as an example. Figure 1 shows the 3D surface and contour plots of the optical field A, the off-diagonal element M, and the population difference F for the same set of initial parameters and different ω values, which are specified in the caption. Here and in what follows, we set the scaled dispersion σ to be 1, without loss of generality. It is clear that as ω increases, the optical field $|A|$ manifests itself as a bright Peregrine soliton, whereas $|M|$ and F exhibit complex dark and bright rogue wave structures that fulfil the spatiotemporally balanced condition (5). Particularly, as $|\kappa| = \frac{2\sqrt{3\sigma a}}{3}$ [see Figs. 1(a) and 1(d)], while $|M|$ has a three-hole structure, the distribution F will take a quite different structure, featuring a single hump as $\kappa = -\frac{2\sqrt{3\sigma a}}{3}$ but a single hole as $\kappa = \frac{2\sqrt{3\sigma a}}{3}$.

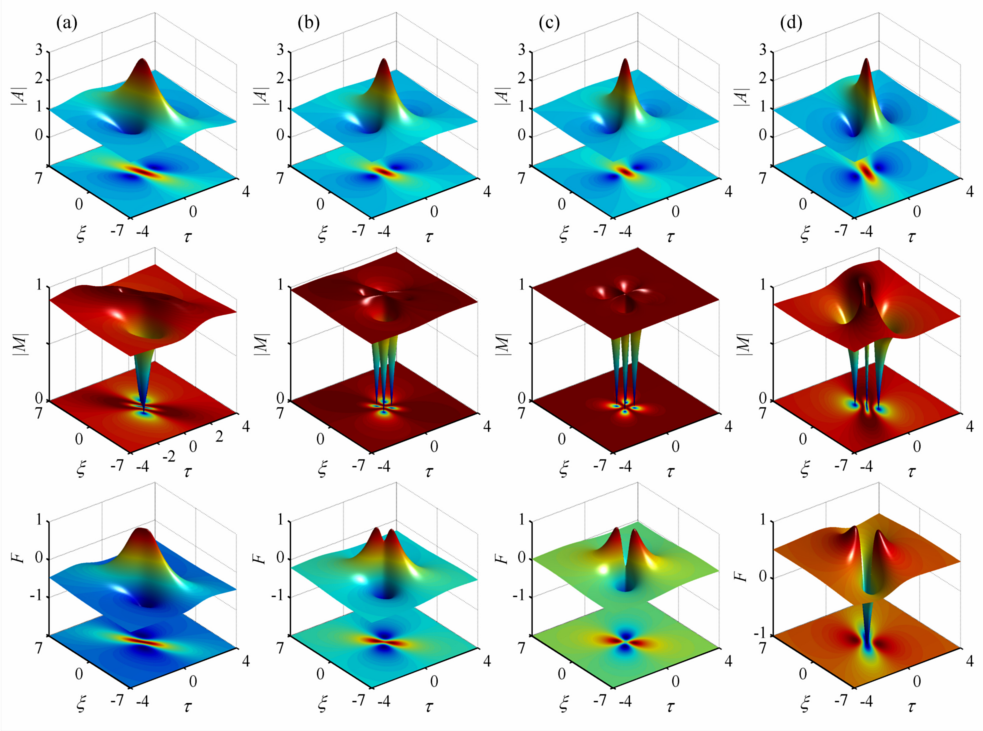

Fig. 1. 3D surface and contour plots of the spatiotemporal evolutions for optical field $|A|$, off-diagonal element $|M|$, population difference F in the MB case ($s = 0$). Column (a): $\omega = \frac{1}{2} - \frac{2\sqrt{3}}{3}$; Column (b): $\omega = 0$; Column (c): $\omega = \frac{1}{2}$; Column (d): $\omega = \frac{1}{2} + \frac{2\sqrt{3}}{3}$. The other parameters are given by $a = 1$, $\sigma = 1$, $\phi = \frac{1}{2}$, and $b = 2a/\sqrt{4\sigma a^2 + \kappa^2}$.

Despite the complexity, these solutions are universal in form, being able to hold for either the MB ($s = 0$) or the NLS-MB ($s = 1$) situation. This is self-evident as the free parameter s only enters into K, η, and χ, see Eqs. (13) and (15). Once the GVD and Kerr effects come into play, the rogue wave structures shown in Fig. 1 still stay, except for a different orientation of the pattern, as shown in the surface and contour plots in Fig. 2, where we used $s = 1$ (NLS–MB case), under otherwise identical parameter condition as in Fig. 1(b).

In fact, the universality of our solutions (9)–(11) can be further confirmed with the higher-order

Optics EXPRESS

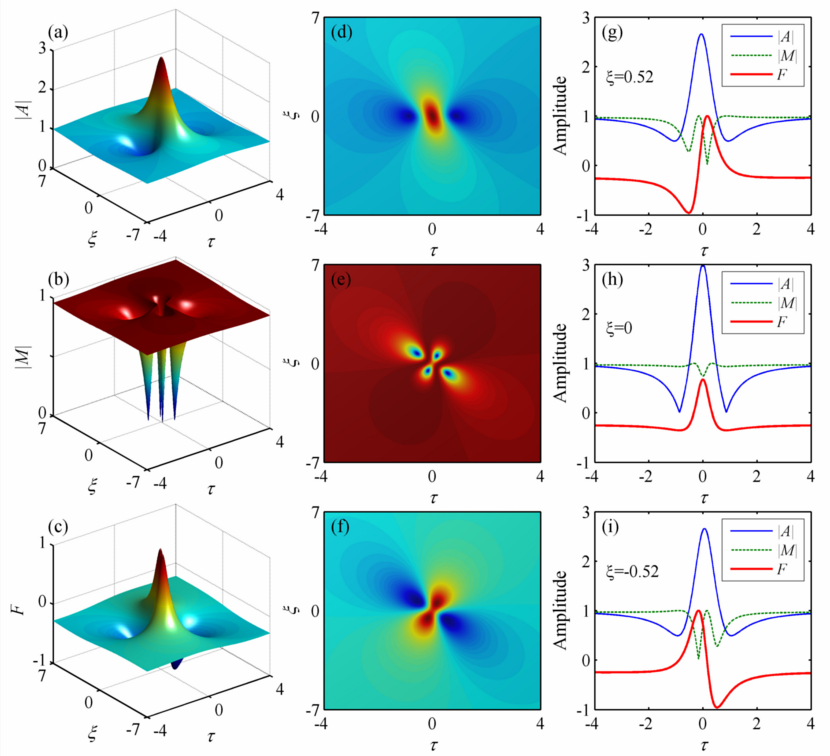

Fig. 2. Spatiotemporal distribution of the rogue wave components $|A|$, $|M|$, and F in the NLS–MB case ($s = 1$) under otherwise identical condition as in Fig. 1(b). (a)–(c): Surface plots; (d)–(f): Contour plots; (g)–(i): Temporal profiles for the amplitudes $|A|$, $|M|$ and the real quantity F at given distances as indicated in the panels.

NLS-MB equations. As an example, for the following Hirota–MB equations [44]:

$$\begin{aligned} A_\xi &= is(\frac{\sigma}{2}A_{\tau\tau} + |A|^2A) + h(\frac{\sigma}{6}A_{\tau\tau\tau} + |A|^2A_\tau) + M, \\ M_\tau &= i\phi M - \frac{2}{\sigma}AF, \\ F_\tau &= M^*A + MA^*, \end{aligned} \tag{20}$$

where σ, s and h are arbitrary real constants, Eqs. (9)–(11) still serve as their fundamental rogue wave solutions, only with the parameters K, η, and χ updated as below

$$K = \frac{b}{a} + s(a^2 - \frac{\sigma\omega^2}{2}) + \frac{h}{6}\omega(6a^2 - \sigma\omega^2), \tag{21}$$

$$\eta = -\frac{\sigma ab}{\kappa^2 + 4\sigma a^2} + \frac{s}{2}a^2 + \frac{h}{2}\omega a^2, \tag{22}$$

$$\chi = \frac{\kappa b}{a(\kappa^2 + 4\sigma a^2)} + s\omega + \frac{h(\sigma\omega^2 - 2a^2)}{2\sigma}. \tag{23}$$

In an analogous manner, our solutions can even be generalized to the infinite NLS hierarchy [17] coupled to the MB equations. This is not surprising because the whole NLS hierarchy share the same linear spectral problem constructed from a loop algebra of $sl(2)$ [10].

Optics EXPRESS

In addition, there would occur a strong population inversion as the optical Peregrine rogue wave interacts with the two-level ions. Specially, an entire inversion could occur as $|\kappa| \leq \frac{2\sqrt{3\sigma}a}{3}$. We note that for complete population inversion, the two-level system needs to be initially prepared slightly beyond the ground state, i.e., $-1 < F_0 < 0$, which requires $\kappa < 0$. Figures 2(g)–2(i) show that for $\kappa = \sigma(\omega - \phi) = -1/2$, it is possible to realize $F = 1$ transiently, namely, an entire population inversion. However, the population inversion usually does not go synchronously with the optical Peregrine pulse, e.g., at $\xi = \pm 0.52$, the value of F reaches unity in the trailing/leading edge, not at the climax, of the optical pulse [see Figs. 2(g) and 2(i)].

5. MI and numerical simulations

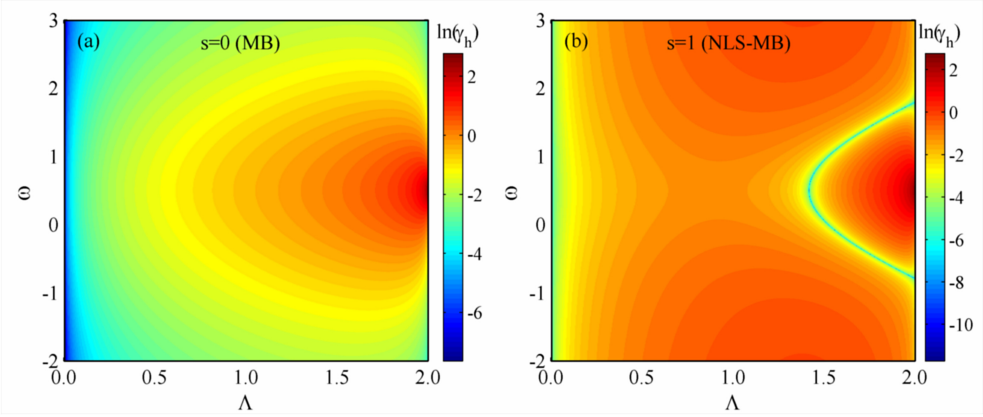

Fig. 3. MI gain map versus Λ and ω: (a) $s = 0$ (MB case); (b) $s = 1$ (NLS–MB case). The other parameters are specified by $a = 1$, $\sigma = 1$, $\phi = \frac{1}{2}$, and $b = 2a/\sqrt{4\sigma a^2 + \kappa^2}$.

Among mechanisms for rogue wave excitation [2], the MI analysis, which uncovers the growth of periodic perturbations on an unstable continuous-wave background, opens a convenient way for understanding and predicting the rogue waves [10, 23, 45]. For our coupled NLS–MB system (8), the plane-wave solutions (14) are perturbed according to $A = A_0\{1 + p_1 \exp[-i\Lambda(\mu\xi - \tau)] + q_1^* \exp[i\Lambda(\mu^*\xi - \tau)]\}$, $M = M_0\{1 + p_2 \exp[-i\Lambda(\mu\xi - \tau)] + q_2^* \exp[i\Lambda(\mu^*\xi - \tau)]\}$, and $F = F_0\{1 + p_3 \exp[-i\Lambda(\mu\xi - \tau)] + p_3^* \exp[i\Lambda(\mu^*\xi - \tau)]\}$, where $p_{1,2,3}$ and $q_{1,2}$ are small amplitudes of the Fourier modes, Λ accounts for the modulation frequency ($\Lambda \geq 0$), and μ is the complex propagation parameter. Substituting these perturbed solutions into Eqs. (8) followed by linearization yields a system of five coupled linear equations for ps and qs. This system has a nontrivial solution only when μ and Λ satisfy the dispersion relation

$$\left[\mu - s\sigma\omega + \frac{b\sigma\kappa}{a(\Lambda^2\sigma^2 - 4a^2\sigma - \kappa^2)}\right]^2 + \frac{\sigma}{4}(4a^2 - \Lambda^2\sigma)\left[s + \frac{2\sigma b}{a(\Lambda^2\sigma^2 - 4a^2\sigma - \kappa^2)}\right]^2 = 0, \quad (24)$$

which is a quadratic equation of μ. It follows that in the baseband limit $\Lambda = 0$, such quadratic equation could always admit complex roots as long as $\sigma > 0$, suggesting that only the anomalous dispersion, if available, permits the formation of rogue waves. This result is identical to that predicted from the analytical solutions (9)–(11).

Figure 3 displays the MI gain maps (in logarithmic scales) associated to Eq. (24), defined by $\ln(\gamma_h) = \ln(\Lambda|\mathrm{Im}(\mu)|)$, versus Λ and ω. It is suggested that the rogue wave solutions would exist in the whole domain of ω, no matter whether $s = 0$ [see Fig. 3(a)] or $s = 1$ [see Fig. 3(b)], as expected above. Nevertheless, a comparison between two maps shows that in general, the

Optics EXPRESS

instability is favored in the NLS-MB case, which means that the rogue wave solution and MI develop effectively over shorter length scales than in the MB case.

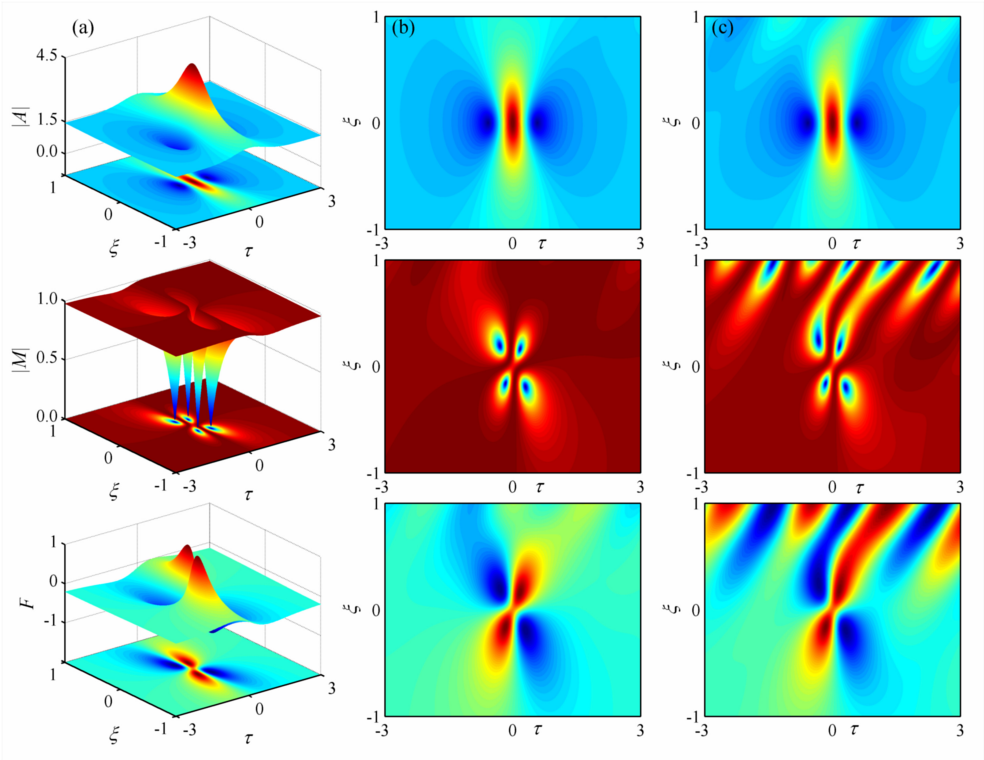

Fig. 4. Evolution of the rogue waves in the NLS-MB case, with $s = 1$, $a = 1.5$, $\sigma = 1$, $\phi = \frac{1}{2}$, and $\omega = 0$. Column (a): Analytical solutions, given by 3D surface and contour plots; Column (b): Contour plots of numerical results, using the analytical solutions (9)–(11) at $\xi = -1$ as initial conditions; Column (c): The numerical results obtained with the solution (9) and the plane waves M_0 and F_0 at $\xi = -1$ as the corresponding initial conditions.

Besides, we study numerically the dynamics and stability of these rogue waves, using the exponential time differencing Crank–Nicolson (ETDCN) scheme with Padé approximation [46], which is proved to be stable and second-order convergent for such kind of stiff problems. To evaluate the dynamics and stability, three numerical games are played, for given system parameters $s = 1$, $a = 1.5$, $\sigma = 1$, $\phi = \frac{1}{2}$, and $\omega = 0$. First, we integrated numerically Eqs. (8) with the analytical solutions (9)–(11) at $\xi = -1$ as initial conditions, and presented the results in the column (b) in Fig. 4. For comparison, the corresponding analytical solutions are provided in Fig. 4(a). It is clear that our numerical code gave precisely the solution profiles predicted analytically until $\xi = 1$. Second, we solved such an underlying model by perturbing significantly the above initial conditions. Specifically, we used the solution (9) at $\xi = -1$ as the initial condition for the optical field component A, while let the matter-wave components M and F take the plane-wave solutions (14), i.e., M_0 and F_0, at $\xi = -1$ as initial values, respectively. These initial conditions correspond to a strong perturbation to analytical solutions. Our simulation results are illustrated in Fig. 4(c). It is shown that the rogue wave structures, particularly for the optical field component, can unfold without significant distortion over a rather long distance, despite the onset of the spontaneous MI which grows exponentially and tends to interfere with the tail of localized solutions. Lastly, in order to see whether these rogue wave solutions would be triggered in

Optics EXPRESS

realistic conditions, we intended to excite them numerically by using the plane-wave solutions (14) at $\xi = 0$, perturbed by small amount of initial white noise, as initial conditions for all three wave components. The results are given in Fig. 5, where the first five distance units have been removed, as hardly any visible changes appear on the chosen scale. It is clearly seen that, after a propagation of 10 distance units or so, the above rogue wave profiles could still be generated from a random wave field; see the wave patterns encircled by a black line.

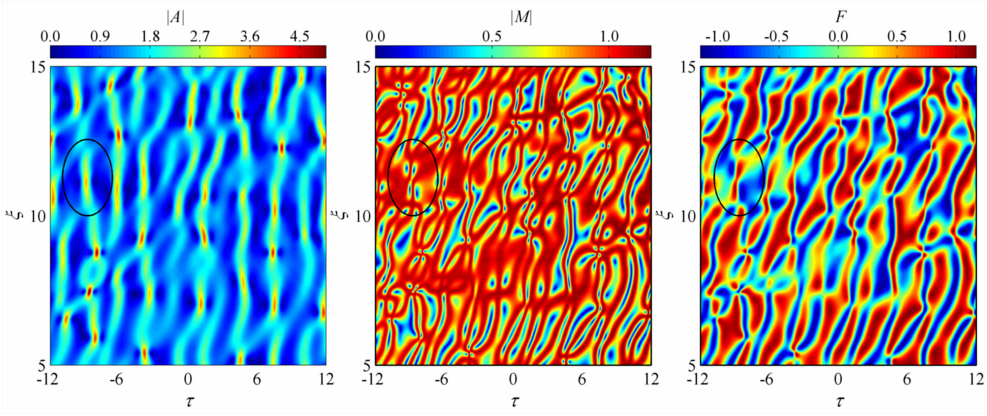

Fig. 5. Numerical excitation of the rogue wave profiles, indicated by the black circles, from a white-noise perturbation to the initial plane-wave solutions (14), under otherwise identical parameter condition as in Fig. 4.

Finally, let us discuss about the possibility of testing experimentally these rogue wave structures. As pointed out in the theoretical investigation from Park and Boyd [29], where the authors considered controlling the signal SIT pulse dynamics by a control field, the neglect of damping processes could be justified by taking the control field to be a continuous wave with a sufficiently large detuning from the resonance or be itself a long SIT soliton pulse, whose duration would be designed to be much larger than the signal SIT pulse but still much shorter than the matter dipole and population relaxation times. The signal SIT pulse would correspond to the Peregrine transient pulse in our case, and the control field to the background wave. An important tradeoff optimization has to be found in that respect, considering that Peregrine solitons develop from an extended background condition— this is the essence of the baseband MI condition for the existence of Peregrine-type rogue waves [45].

Then, considering the erbium-doped fiber as a suitable propagation medium candidate, we know from the seminal experiments performed by Nakazawa *et al.* [41] that the cooling of the gain fiber to the cryogenic temperature of 4.2 K is a prerequisite to increase the dipole decay time to nanoseconds. Using modern optical pulse waveform generators, it should be possible to prepare an effective though truncated background condition, leading to a reasonably good approximation of the vector rogue wave dynamics described in the present paper. Although the parameter condition (7) seems to be stringent, it is indeed able to be achieved via the dispersion engineering and management [47] as well as the modification of the transition electric dipole moment of doping ions [31]. Whereas the recording of the optical component features down to a few tens of picosecond could be performed with ultrafast optical measurement techniques [48], the observation of its matter-wave counterpart would remain particularly challenging.

Optics EXPRESS

6. Conclusion

In conclusion, we studied the resonant interaction of an optical field with two-level doping ions in a cryogenic optical fiber within the framework of NLS-MB equations. We presented exact explicit fundamental rational rogue wave solutions for the coupled optical and matter waves. It was exhibited that the optical wave component always features a typical Peregrine-like structure, while the matter waves involve more complicated yet spatiotemporally balanced amplitude distribution. The existence and stability of these rogue waves was then confirmed by numerical simulations. Moreover, the rogue waves were shown to be excited from a noisy initial condition, amid the onset of MI. These solutions can also be extended, using the same analytical framework, to include higher-order dispersive and nonlinear effects, highlighting their universality. Finally, in the light of the recurrence stability of these rogue waves from chaotic wave fields, we discuss the possibility of their experimental observation, by providing a clearer access to the parameters needed for experimental design.

Funding

National Natural Science Foundation of China (NSFC) (11174050, 11474051); Horizon 2020 Framework Programme (740355); IFCPAR/CEFIPRA (5104-2); Program for Professor of Special Appointment at Shanghai Institutions of Higher Learning (TP2014046).